Quantum magnetization discontinuities proportional in number to the spin s in C_{60}

N. P. Konstantinidis[1]

1 Department of Mathematics and Natural Sciences, The American University of Iraq, Sulaimani, Kirkuk Main Road, Sulaymaniyah, Kurdistan Region, Iraq
* npknpk1111@gmail.com

December 5, 2022

Abstract

The antiferromagnetic Heisenberg model on the fullerene C_{60} in a magnetic field has $4s$ ground-state magnetization discontinuities as a function of the spin quantum number s that disappear at the classical limit. The molecule can be seen as the fullerene C_{20} with interpentagonal interactions that can be tuned to generate the discontinuities. The results show how spatial symmetry dictates the magnetic response of the I_h fullerene molecules.

Contents

1 Introduction

Fullerenes are allotropes of carbon whose most representative member is C_{60} [1–9]. C_{60} superconducts when doped with alkali metals [10]. Electron correlations are important for doped C_{60}, and they are accurately described within the framework of the Hubbard model (see [11] and references therein). According to estimates for the on-site repulsion U, C_{60} belongs to the intermediate-U regime of the Hubbard model [12–15], but its large U-limit, the Heisenberg model, is expected to qualitatively capture the spin correlations [16].

In the antiferromagnetic Heisenberg model the total magnetization along an external field axis S^z changes discontinuously at specific field values typically by $\Delta S^z = 1$. In cases of spin-space anisotropy the energy is more efficiently minimized along certain directions, and this can lead to discontinuities with $\Delta S^z > 1$. It is of particular interest when such magnetization discontinuities occur in the absence of magnetic anisotropy. These are solely due to the frustrated connectivity of the magnetic interactions, directly reflecting the topology of the structure hosting the magnetic units.

The antiferromagnetic Heisenberg model has been extensively used to model the magnetic properties of low-dimensional frustrated topologies [17–22]. In fullerene molecules frustration is introduced by the twelve pentagons that each molecule has, with the number of hexagons increasing linearly with size [1]. The most symmetric fullerene molecules have I_h symmetry like C_{60}. These are minimally frustrated among the fullerenes if one excludes the Platonic solid dodecahedron [23–26] that only has pentagons [27, 28], and have also been found to share the ground-state magnetic response. At the classical level there are two magnetization discontinuities in an external field when all exchange interactions are equal, with the exception of the dodecahedron that has three [16, 29, 30]. In the extreme quantum limit where the individual spin magnitude $s = \frac{1}{2}$ and 1, the dodecahedron has respectively one and two discontinuities [29]. A high-field ground-state magnetization jump was established to be a common feature of the I_h fullerenes for $s = \frac{1}{2}$ when all exchange interactions are equal [30]. Relatively small fullerene molecules with different symmetry have only pronounced magnetization plateaus when $s = \frac{1}{2}$ [31, 32]. Magnetization discontinuities have also been observed in the case of extended systems [33–40].

The dual of the dodecahedron, the icosahedron, has also been shown to possess a magnetization discontinuity at the classical lowest-energy configuration in an external field, which disappears at the extreme quantum limit [41]. This discontinuity can be understood from a structural point of view, as the icosahedron can be viewed as a closed strip of a triangular lattice with two additional spins attached [42]. Such a structural explanation of the magnetization discontinuities is not obvious for the dodecahedron. It can neither apply to the discontinuities of fullerene molecules where all pentagons are located at their ends and their body has the form of a nanotube, comprising only of hexagons [11].

To investigate the origin of the magnetization discontinuity of the dodecahedron for $s = \frac{1}{2}$ and 1 the anisotropic Heisenberg model (AHM) is considered. Its antiferromagnetic isotropic limit is approached from the corresponding Ising limit by gradually increasing the strength of the interactions in the xy plane. This was first done by Karľová *et al.* for $s = \frac{1}{2}$ [43]. They showed that the discontinuity at the isotropic limit originates in a discontinuity at the saturation field in the Ising limit, with the former evolving continuously from the latter. In this paper the ground-state discontinuity of the antiferromagnetic Ising limit is more closely monitored as the fluctuations in the xy plane are switched on. Perturbation theory on the xy-plane interactions shows that the saturation-field jump at the Ising limit develops into the high-field magnetization discontinuity five spin-flips away from saturation for any finite s, with the discontinuity disappearing at the classical limit $s \to \infty$, demonstrating its pure quantum nature. Then evolving continuously away from the antiferromagnetic Ising limit by increasing the strength of the xy coupling shows that the jump survives beyond the isotropic Heisenberg limit for $s = \frac{1}{2}$ and 1. For increasingly higher s the fluctuations are strong enough to confine the discontinuity closer and closer to the Ising limit.

The calculation is then extended to the next-bigger I_h fullerene, the truncated icosahedron C_{60}, which has also been found to support the magnetization discontinuity five spin flips away from saturation for $s = \frac{1}{2}$ and uniform interactions [30]. Here the relative strength of the two symmetrically independent interactions is allowed to vary and controls how strongly neighboring pentagons are coupled, since they are isolated from one another and do not share any

vertices or edges, as in the dodecahedron. Perturbation theory shows that the discontinuity is again generated infinitesimally away from the antiferromagnetic Ising limit for arbitrary s, but its existence at the antiferromagnetic isotropic limit depends on the interpentagonal coupling, which must be made roughly equal to the intrapentagonal one in order for the discontinuity to survive for $s = \frac{1}{2}$. Increasing s again works against the discontinuity, but making the interpentagonal coupling strong enough allows the jump to appear for arbitrary s, with the required minimum interpentagonal coupling increasing with s and the AHM approaching closer and closer its strong interpentagonal or dimer limit. This demonstrates that the interactions can be tuned in order for C_{60} to behave like its smaller symmetric relative, C_{20}, and shows the close connection between symmetry and magnetic properties.

In order to investigate in more detail the behavior close to the dimer limit where the discontinuity is favored and the interpentagonal is much stronger than the intrapentagonal interaction, perturbation theory on the latter is considered for arbitrary s. This calculation can be performed for the whole S^z range as long as s is not too big. C_{60} then reduces to an icosidodecahedron of dimers interacting weakly with one another. For $s = \frac{1}{2}$ it is found that apart from the five-spin-flips away from saturation discontinuity at the isotropic AHM limit, another one exists at low fields with the $S^z = 5$ sector never including the ground state in a field. This is a manifestation of the singlet-triplet or hole-particle symmetry between low and high magnetic fields after the projection to the lowest-energy singlet and triplet states of the dimers has been made [44–46]. Perturbation theory for arbitrary s shows that the number of discontinuities grows as $4s$, with the pattern of lower and higher-field jumps repeating in the magnetization curve $2s$ times and disappearing at the classical limit. These discontinuities are expected to survive away from the dimer limit, as has been shown for the one close to saturation, and demonstrate the rich magnetic response of C_{60}. Since symmetry and strong interpentagonal coupling are important for the appearance of the jumps, it is expected that they will be general features of the I_h-fullerene molecules, as has already been demonstrated for the discontinuity close to saturation [30].

2 Model

The Hamiltonian of the AHM in a magnetic field h with a single spin $\vec{s}_i$, $i = 1, \ldots, N$ located on each of the N vertices of a molecule is

$$H = \sum_{<ij>} J_{ij}[sin\omega(s_i^x s_j^x + s_i^y s_j^y) + cos\omega s_i^z s_j^z] - h\sum_{i=1}^{N} s_i^z \tag{1}$$

The symbol <> indicates that interactions are limited to nearest-neighbors and have strength equal to J_{ij} for spins i and j. The Ising coupling along the z axis is scaled with $cos\omega$ and the coupling in the xy plane with $sin\omega$, with $0 \leq \omega \leq \frac{3}{4}\pi$. The antiferromagnetic limits are the Ising for $\omega = 0$, the isotropic Heisenberg for $\omega = \frac{\pi}{4}$, and the XX for $\omega = \frac{\pi}{2}$. The interactions are taken to obey the molecular symmetry, with two edges connected by a symmetry operation of the I_h point group corresponding to the same interaction strength. The magnetic field is directed along the z axis. Hamiltonian (1) is block-diagonalized by taking into account S^z and its spatial and spin symmetries [29]. It is also possible to perturb away from the Ising limit of Hamiltonian (1) with the interactions in the xy plane by simultaneously taking its symmetries into account.

3 Dodecahedron C_{20}

The dodecahedron is a Platonic solid [23], and all its $N = 20$ vertices are geometrically equivalent. It consists of twelve pentagons, and is the smallest fullerene in the form of C_{20} [1,24–26]. All of its edges are symmetrically equivalent, making all bonds J_{ij} in Hamiltonian (1) equal. At the antiferromagnetic Ising limit $\omega = 0$ the lowest energy of Hamiltonian (1) belongs to both the $S^z = 0$ and $4s$ subsectors, making the lowest-lying levels from $S^z = 1$ to $4s-1$ excited (Tables 1, 2, and 3). The ground-state energy as a function of S^z is linear, resulting in a strong magnetization jump $\Delta S^z = 16s$ to saturation (Figs 1 and 2).

Table 1: Hamiltonian (1) with $h = 0$ for C_{20} for $s = \frac{1}{2}$. The columns list the sector S^z, the lowest energy E_0 at the Ising limit $\omega = 0$, its degeneracy (deg.), the first-order perturbation theory energy correction E_1 on ω, its degeneracy (deg.), and the irreducible representation (irrep.) of the I_h symmetry group it belongs. E_1 has been calculated with double-precision accuracy but less digits are shown.

S^z	E_0	deg.	E_1	deg.	irrep.
0	$-\frac{9}{2}$	240	$-(\sqrt{3}+\frac{1}{2})$	1	A_u
1	-4	900	-2.64146	3	T_{2u}
2	$-\frac{9}{2}$	5	0	5	A_g, F_g
3	-3	320	-2.56533	4	F_u
4	$-\frac{3}{2}$	1240	-3.68687	1	A_g
5	0	1912	-3.54419	4	F_g
6	$\frac{3}{2}$	1510	-3.59294	1	A_u
7	3	660	-3.02938	3	T_{1u}
8	$\frac{9}{2}$	160	-2.13276	5	H_g
9	6	20	$-\frac{\sqrt{5}}{2}$	3	T_{2u}
10	$\frac{15}{2}$	1	0	1	A_g

Perturbing away from the Ising limit with the interactions in the xy plane in first order ($\omega \to 0$) decreases the $S^z = 0$-energy but not the $S^z = 4s$ for $s = \frac{1}{2}$ (Table 1), resulting in a low-field $\Delta S^z = 4s$ magnetization jump (Fig. 1). For $s = 1$ and $\frac{3}{2}$ first-order perturbation theory does not resolve this degeneracy (Tables 2 and 3), but the full calculation shows that the low-field $\Delta S^z = 4s$ discontinuity also occurs when $s = 1$ (Fig. 2). Magnetization jumps occur when the energy differences between successive S^z sectors do not increase with increasing S^z. That first-order perturbation theory can not resolve the degeneracies away from the high-S^z region is also demonstrated by the degeneracy of the energy corrections in Tables 2 and 3, which belong to multiple irreducible representations [47]. First-order perturbation theory shows the existence of a magnetization jump between $4s$ and $Ns-6$ for $s = 1$ and $\frac{3}{2}$. Fig. 2 shows that the jump survives for higher values of ω for $s = 1$.

In contrast to what happens for lower S^z, from $S^z = Ns-6$ to saturation the ground states belong to a single irreducible representation, which does not change with increasing s. The first-order perturbative corrections in these S^z sectors are multiples of s (Table 4), making the magnetization response close to saturation the same for any s. Calculating the energy differences between the high-field successive sectors shows that the $S^z = Ns-5$ sector, the one with five spin-flips away from saturation, never becomes the ground state in the field, irrespective of s. The energy differences between the sectors scale with s, while the energies at the classical limit scale as s^2, showing that the discontinuity is a pure quantum effect which occurs for arbitrary finite s, but disappears at the classical limit $s \to \infty$.

Table 2: Same as Tab. 1 for $s = 1$.

S^z	E_0	deg.	E_1	deg.	irrep.	S^z	E_0	deg.	E_1	deg.	irrep.
0	-18	240	0	240	all	11	3	41120	-4.20815	30	all but A_g,A_u
1	-17	1440	-2	60	all but A_g	12	6	41475	-5.22625	10	A_g,F_g,H_g
2	-16	4080	-3.81284	30	all but T_{1g},T_{2g},A_u	13	9	32920	-6.25465	20	A_g,F_g,H_g, T_{1u},T_{2u},F_u
3	-17	60	-1	30	all but A_g,A_u	14	12	20520	-7.37374	1	A_g
4	-18	5	0	5	A_g,F_g	15	15	9932	-7.08838	4	F_g
5	-15	40	0	40	all	16	18	3650	-7.18588	1	A_u
6	-12	460	0	460	all	17	21	980	-6.05876	3	T_{1u}
7	-9	2520	$-\sqrt{2}$	60	all but A_u	18	24	180	-4.26553	5	H_g
8	-6	8310	$-\sqrt{5}$	120	all	19	27	20	$-\sqrt{5}$	3	T_{2u}
9	-3	18920	-3.12602	40	all	20	30	1	0	1	A_g
10	0	31852	-3.62611	120	all						

The dodecahedron is small enough to calculate the lowest-energy eigenvalues in each S^z-sector for $s = \frac{1}{2}$ and 1, allowing to monitor the evolution of all magnetization discontinuities away from first-order perturbation theory on the antiferromagnetic Ising limit. The magnetization response for $s = \frac{1}{2}$ and 1 is shown in Figs 1 and 2. Karľová *et al.* have provided the plot for $s = \frac{1}{2}$ up to $\omega = \frac{\pi}{4}$ [43]. As the coupling in the xy plane gets stronger the high-field discontinuity survives at the isotropic Heisenberg limit $\omega = \frac{\pi}{4}$ for both values of s. The other discontinuities disappear, with the exception of a $\Delta S^z = 2$ discontinuity around $S^z = 9$ for $s = 1$, that reenters a little before the isotropic limit and traces back to the $\Delta S^z = 10$ discontinuity of weak ω.

Monitoring the discontinuities away from the isotropic limit for higher ω shows that the two $s = 1$ jumps quickly disappear, while the $s = \frac{1}{2}$ discontinuity survives up to the XX limit where $\omega = \frac{\pi}{2}$ and the Ising interaction is zero. Further increasing ω makes the interaction along the z axis ferromagnetic, and eventually the discontinuity disappears at $\omega = 0.68562\pi$. The detrimental effect of the xy-plane fluctuations on the high-field discontinuity away from the Ising limit is getting stronger with s as shown in Fig. 3, which plots the highest ω value for which the jump survives as a function of s (Table 5). The jump does not survive at the isotropic Heisenberg limit for $s > 1$.

4 Truncated Icosahedron C_{60}

The truncated icosahedron has $N = 60$ and is an Archimedean solid [48], having all vertices geometrically equivalent and two different types of polygons, pentagons and hexagons. It is the most representative fullerene in the form of C_{60} [1–8]. It has two symmetrically unique types of edges, which correspond to two independent exchange interactions in Hamiltonian (1). The first type links vertices of the same pentagon and is taken to have strength $cos\phi$, while the second vertices that belong to different pentagons and has strength $sin\phi$, with $0 \leq \phi \leq \frac{\pi}{2}$, interpolating between isolated pentagons and isolated dimers. Unlike the dodecahedron the pentagons do not share vertices but rather interact via the interpentagon bonds, which allow control of the interaction strength between neighboring pentagons.

Table 3: Same as Tab. 1 for $s = \frac{3}{2}$.

S^z	E_0	deg.	E_1	deg.	irrep.	S^z	E_0	deg.	E_1	deg.	irrep.
0	-40.5	240	0	240	all	16	4.5	250840	-4.78375	30	all but T_{1g},T_{2g},A_u
1	-39	1440	$-\frac{3}{2}$	720	all	17	9	301680	-5.43916	120	all
2	-37.5	4320	-3	720	all	18	13.5	320160	-6.24360	120	all
3	-36	9980	$-\frac{9}{2}$	340	all	19	18	300400	-6.31222	30	all but A_g,A_u
4	-37.5	360	-3	75	all	20	22.5	249032	-7.83938	10	A_g,F_g,H_g
5	-39	60	$-\frac{3}{2}$	30	all but A_g,A_u	21 21	27 27	181860 181860	-7.83938 -7.83938	20 20	A_g,F_g,H_g T_{1u},T_{2u},F_u
6	-40.5	5	0	5	A_g,F_g	22	31.5	116315	-9.38197	20	A_g,F_g,H_g T_{1u},T_{2u},F_u
7	-36	40	0	40	all	23	36	64560	-9.38197	20	A_g,F_g,H_g T_{1u},T_{2u},F_u
8	-31.5	180	0	180	all	24	40.5	30680	-11.06061	1	A_g
9	-27	880	0	880	all	25	45	12232	-10.63257	4	F_g
10	-22.5	3570	0	3570	all	26	49.5	3970	-10.77881	1	A_u
11	-18	11480	$-\frac{3}{2}\sqrt{2}$	60	all but A_u	27	54	1000	-9.08814	3	T_{1u}
12	-13.5	29800	$-\frac{3}{2}\sqrt{2}$	360	all	28	58.5	180	-6.39829	5	H_g
13	-9	64040	$-\frac{3}{2}\sqrt{5}$	120	all	29	63	20	$-\frac{3}{2}\sqrt{5}$	3	T_{2u}
14	-4.5	116695	$-\frac{3}{2}\sqrt{5}$	600	all	30	67.5	1	0	1	A_g
15	0	183232	-4.68903	40	all						

Table 6 lists the first-order perturbation theory corrections away from the antiferromagnetic Ising limit $\omega = 0$ for arbitrary s, three values of ϕ and higher S^z. Like the dodecahedron, the sector with five spin-flips from saturation is never the ground state in a magnetic field. The discontinuity of the dodecahedron is inherited from the truncated icosahedron, which shares its spatial symmetry, irrespectively of the relative strength of the two symmetrically unique exchange interactions. Further evidence to that is provided by the irreducible representations that include the lowest-energy state in each S^z sector, which are very similar for the two molecules.

For the dodecahedron it was found that the fluctuations around the Ising axis work against the high-field magnetization discontinuity, and eventually a sufficiently strong value of ω makes the discontinuity disappear. The same is true for the truncated icosahedron, and Fig. 4 plots the maximum value ω_{max} for which the high-field magnetization discontinuity exists as a function of ϕ for s up to $\frac{3}{2}$ (the corresponding data is listed in Table 7). For weak ϕ neighboring pentagons are weakly coupled and ω_{max} is small and slightly decreases with ϕ. As ϕ increases the interpentagon bonds get stronger at the expense of the intrapentagon bonds, resulting in a discontinuity that survives up to higher values of ω, until a sufficiently strong ϕ supports the jump up to the isotropic limit $\omega = \frac{\pi}{4}$.

The ω_{max} value for which the discontinuity survives decreases with s for fixed ϕ according to Fig. 4, showing that quantum fluctuations are detrimental to the jump, as has also been found for the dodecahedron. Simultaneously, the required ϕ value for the jump to survive at the Heisenberg limit increases with s, and is already close to $\frac{\pi}{2}$ for $s = \frac{3}{2}$. These results demonstrate that the stronger the interaction between the pentagons the more "dodecahedron-like" the truncated icosahedron becomes in terms of discontinuous magnetic response, and that

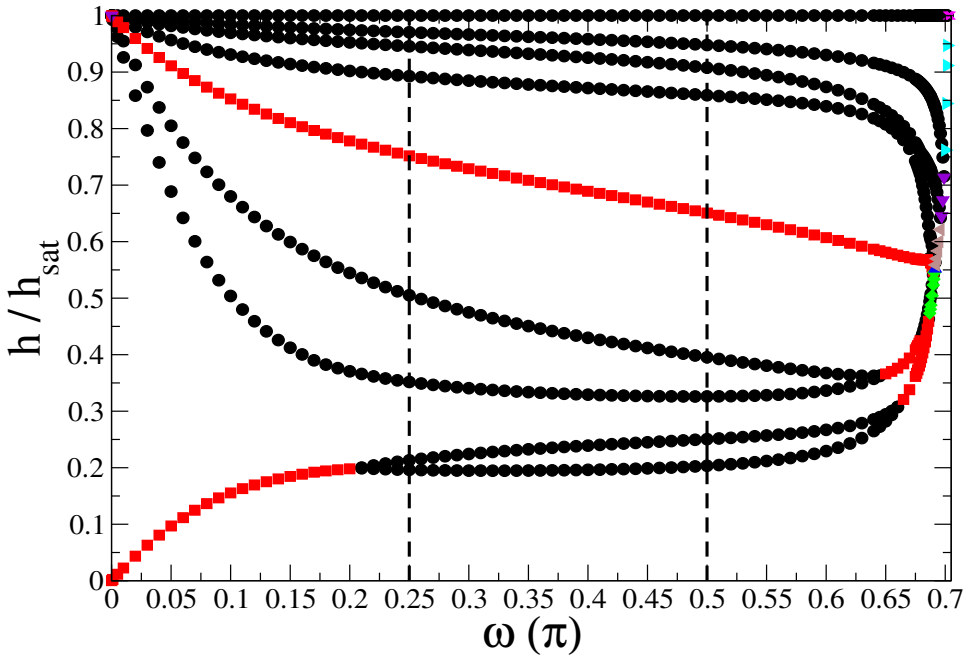

Figure 1: Magnetic fields h over the saturation field h_{sat} for which ground-state magnetization discontinuities occur as a function of ω in the ground state of Hamiltonian (1) for C_{20} for $s = \frac{1}{2}$. The (black) circles correspond to discontinuities with $\Delta S^z = 1$, the (red) squares with $\Delta S^z = 2$, the (green) diamonds with $\Delta S^z = 3$, the (blue) triangles up with $\Delta S^z = 6$, the (brown) triangles left with $\Delta S^z = 7$, the (violet) triangles down with $\Delta S^z = 8$, the (cyan) triangles right with $\Delta S^z = 9$, and the (magenta) X's with $\Delta S^z = 10$. The (black) dashed lines show the Heisenberg ($\omega = \frac{\pi}{4}$) and the XX ($\omega = \frac{\pi}{2}$) limit.

the interpentagon interactions provide a controlled way to tune the magnetic behavior of the molecule. They also explain the common magnetic properties of the two molecules, and also point to a similar mechanism for bigger I_h fullerenes that also share these properties [30]. In their case the interpentagon interaction is effected by more than one exchange interactions [1].

The inset of Fig. 4 focuses on values of ϕ close to $\frac{\pi}{2}$. Contrary to what happens for smaller ϕ, ω_{max} increases with s as ϕ approaches $\frac{\pi}{2}$. At the limit $\phi \to \frac{\pi}{2}$ the truncated icosahedron reduces to 30 dimers perturbatively coupled via intrapentagon bonds, which form an icosidodecahedron. First-order perturbation theory gives the lowest-energy correction at the Heisenberg limit $\omega = \frac{\pi}{2}$ for every S^z sector as long as s is not too big (Tables 8, 9, and 10). There are $4s$ discontinuities as a function of s, with the sectors $S^z = \frac{N}{2}i+5$ and $S^z = \frac{N}{2}(i+1)-5$ with $i = 0, 1, \ldots, 2s-1$ never including the ground state in a magnetic field. These are sectors with an S^z value differing by 5 from sectors whose S^z is an integer multiple of $\frac{N}{2}$. The appearance of discontinuities in pairs for regions of S^z where $\frac{N}{2}i \leq S^z \leq \frac{N}{2}(i+1)$ originates in the hole-particle symmetry with respect to the center of the region, after the projection to the lowest-energy dimer states has been made (App. A) [44–46]. Table 11 lists the ω_{max} values for the different discontinuities when $\phi \to \frac{\pi}{2}$, which increase with s as was also found in the inset of Fig. 4.

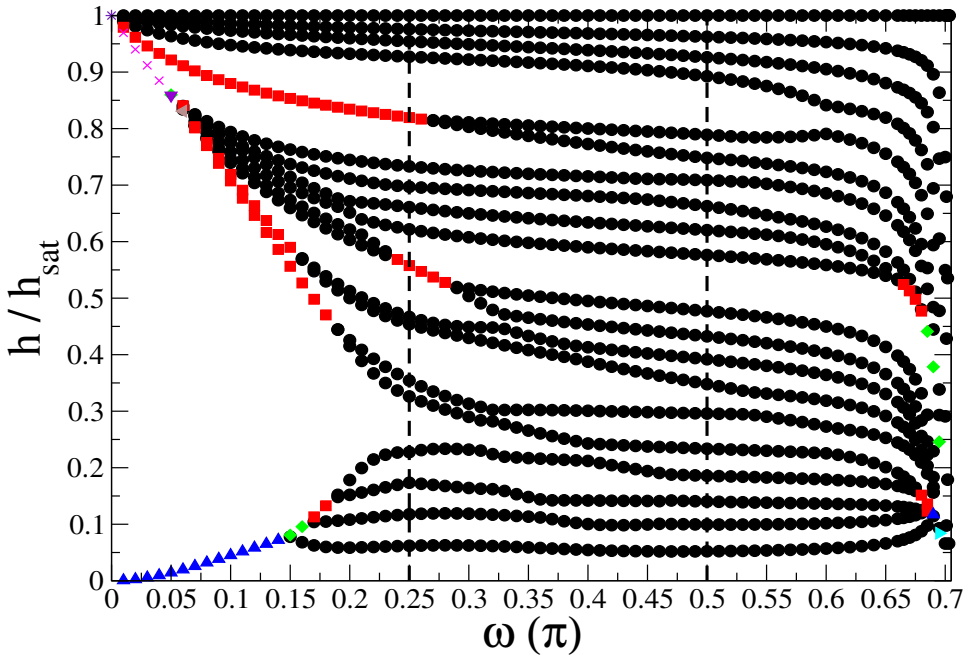

Figure 2: Magnetic fields h over the saturation field h_{sat} for which ground-state magnetization discontinuities occur as a function of ω in the ground state of Hamiltonian (1) for C_{20} for $s = 1$. The (black) circles correspond to discontinuities with $\Delta S^z = 1$, the (red) squares with $\Delta S^z = 2$, the (green) diamonds with $\Delta S^z = 3$, the (blue) triangles up with $\Delta S^z = 4$, the (brown) triangles left with $\Delta S^z = 6$, the (violet) triangles down with $\Delta S^z = 7$, the (cyan) triangles right with $\Delta S^z = 9$, the (magenta) X's with $\Delta S^z = 10$, and the (indigo) stars with $\Delta S^z = 16$. The (black) dashed lines show the Heisenberg ($\omega = \frac{\pi}{4}$) and the XX ($\omega = \frac{\pi}{2}$) limit.

5 Conclusions

In this paper it was shown that the quantum magnetization discontinuity of the isotropic antiferromagnetic Heisenberg model on C_{20} in an external field can be continuously traced to a strong discontinuity present at the Ising limit of the model for finite s. This discontinuity originates in the special connectivity of the dodecahedron. C_{60}, which also has I_h symmetry, inherits the discontinuity at the isotropic limit as the interaction strength of its twelve pentagons can be controlled with the interpentagon interactions. If the latter are made sufficiently strong then the number of discontinuities is shown to be $4s$, and these discontinuities are expected to survive at least close to the dimer limit.

Since the $N = 80$ I_h-symmetry fullerene (chamfered dodecahedron) [1] also has a jump in a magnetic field for $s = \frac{1}{2}$ when its two symmetrically unique interactions are equal [30], it is expected that bigger molecules with the same symmetry will follow the discontinuity pattern of C_{60}. In their case the interpentagonal coupling can also be controlled by tuning the strength of exchange interactions of one or more kinds.

The results of the paper show how the magnetization response is determined by the spatial symmetry for the I_h fullerene molecules. The twelve pentagons are distributed according to a specific symmetry that is directly connected with how the spins react to an external magnetic field. Such common magnetic behavior of a molecular family is well sought-after [11, 27, 29, 30, 49, 50].

Table 4: Hamiltonian (1) with $h = 0$ for C_{20} for arbitrary s. The columns list the sector S^z, the first-order perturbation theory energy correction per spin magnitude $\frac{E_1}{s}$ on ω (away from the Ising limit $\omega = 0$), its degeneracy (deg.), and the irreducible representation (irrep.) of the I_h symmetry group it belongs. E_1 has been calculated with double-precision accuracy but less digits are shown.

S^z	$\frac{E_1}{s}$	deg.	irrep.
$Ns-6$	-7.37374	1	A_g
$Ns-5$	-7.08838	4	F_g
$Ns-4$	-7.18588	1	A_u
$Ns-3$	-6.05876	3	T_{1u}
$Ns-2$	-4.26553	5	H_g
$Ns-1$	$-\sqrt{5}$	3	T_{2u}
Ns	0	1	A_g

Table 5: Maximum value ω_{max} for different s for which the ground state of Hamiltonian (1) for C_{20} has a magnetization discontinuity between $S^z = Ns-6$ and $Ns-4$. The jump does not survive at the isotropic Heisenberg limit $\omega = \frac{\pi}{4}$ for $s > 1$.

s	$\omega_{max}(\pi)$
$\frac{1}{2}$	0.68562
1	0.26685
$\frac{3}{2}$	0.12745
2	0.08186
$\frac{5}{2}$	0.06007
3	0.04739

A Perturbation Theory on the Interpentagon Coupling for C_{60}

As an example, the case $s = 1$ is considered. The interaction between spins belonging to different pentagons is given by the term inside the brackets in Hamiltonian (1) with $0 \leq \omega \leq \frac{3}{4}\pi$, and the lowest energies of these dimers in the different dimer-S^z sectors are

$$\begin{aligned} S^z = 0 \quad & e_0 = -\tfrac{1}{2}(cos\omega + \sqrt{1+7sin^2\omega}) \\ S^z = 1 \quad & e_1 = -sin\omega \\ S^z = 2 \quad & e_2 = cos\omega \end{aligned} \tag{2}$$

It is $e_0 < e_1 < e_2$ for $0 \leq \omega < \frac{3}{4}\pi$. The corresponding eigenstates are called $|0>$, $|1>$, and $|2>$ respectively. The unperturbed Hamiltonian (1) at the $\phi = \frac{\pi}{2}$-limit for C_{60} includes only the interpentagon bonds, resulting in isolated dimers. The representatives of the lowest-energy unperturbed states as a function of S^z are given as sets of the number of dimers found in the three different dimer eigenstates (# in $|0>$,# in $|1>$,# in $|2>$) $= (n_0, n_1, n_2)$:

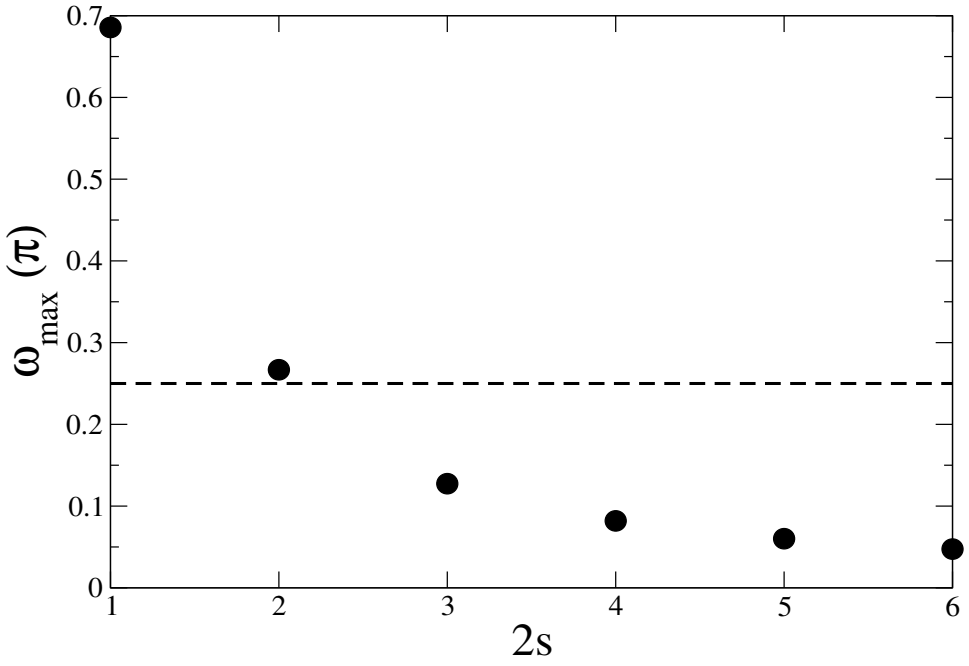

Figure 3: Maximum value ω_{max} as a function of s for which the ground state of Hamiltonian (1) for C_{20} has a magnetization discontinuity five spin flips away from saturation. The dashed line shows the Heisenberg limit.

S^z	dimer eigenstate types	number of states
60	$(0,0,60)$	1
59	$(0,1,59)$	30
58	$(0,2,58)$	435
57	$(0,3,57)$	4060
56	$(0,4,56)$	27405
55	$(0,5,55)$	142506
54	$(0,6,54)$	593775
⋮	⋮	⋮
32	$(0,58,2)$	435
31	$(0,59,1)$	30
30	$(0,60,0)$	1
29	$(1,59,0)$	30
28	$(2,58,0)$	435
27	$(3,57,0)$	4060
26	$(4,56,0)$	27405
25	$(5,55,0)$	142506
24	$(6,54,0)$	593775
⋮	⋮	⋮
2	$(58,2,0)$	435
1	$(59,1,0)$	30
0	$(60,0,0)$	1

(3)

Table 6: Hamiltonian (1) with $h = 0$ for C_{60} for arbitrary s and three different values of ϕ that determines the relative strength of the symmetrically independent exchange interactions. The columns list the sector S^z, and for each ϕ value the first-order perturbation theory energy correction per spin magnitude $\frac{E_1}{s}$ on ω (away from the Ising limit $\omega = 0$), its degeneracy (deg.), and the irreducible representation (irrep.) of the I_h symmetry group it belongs. E_1 has been calculated with double-precision accuracy but less digits are shown.

	$\phi = \frac{\pi}{100}$			$\phi = \frac{\pi}{4}$			$\phi = \frac{49}{100}\pi$		
S^z	$\frac{E_1}{s}$	deg.	irrep.	$\frac{E_1}{s}$	deg.	irrep.	$\frac{E_1}{s}$	deg.	irrep.
$Ns-7$	-11.34792	4	F_u	-11.43936	4	F_u	-7.19164	4	F_u
$Ns-6$	-9.79862	1	A_g	-10.22177	1	A_g	-6.20833	1	A_g
$Ns-5$	-8.18714	4	F_u	-8.69749	3	T_{1g}	-5.19086	4	F_u
$Ns-4$	-6.57530	1	A_u	-7.19834	1	A_u	-4.17734	1	A_u
$Ns-3$	-4.93832	3	T_{1g}	-5.46684	3	T_{1g}	-3.14149	3	T_{1g}
$Ns-2$	-3.29478	5	H_g	-3.67399	5	H_g	-2.09766	5	H_g
$Ns-1$	-1.64865	3	T_{2g}	-1.85123	3	T_{2g}	-1.05033	3	T_{2g}
Ns	0	1	A_g	0	1	A_g	0	1	A_g

The corresponding unperturbed energies are $E_0(S^z) = n_0e_0 + n_1e_1 + n_2e_2$. Interdimer interactions, which are nearest-neighbor pentagon interactions, are taken as a perturbation to the $\phi = \frac{\pi}{2}$-limit of Hamiltonian (1). Tables 8, 9, and 10 list the first-order perturbation theory energy corrections of the interpentagon bonds on the $\phi = \frac{\pi}{2}$-dimer limit Hamiltonian (1) for $s = \frac{1}{2}$, 1, and $\frac{3}{2}$ at the Heisenberg limit $\omega = \frac{\pi}{4}$.

Within first-order perturbation theory the lowest-energy levels in the different S^z sectors are given as $E_0(S^z) + E_1(S^z)\lambda$, with λ the perturbation parameter away from the dimer limit. The difference between successive unperturbed energies is the same for $\frac{N}{2}i \le S^z \le \frac{N}{2}(i+1)$, $i = 0, 1, \ldots, 2s-1$. At the borders between these $2s$ regions the magnetization step $\Delta S^z = 1$. Within first-order perturbation theory the magnitude of ΔS^z within the $2s$ regions is determined by the difference in the energies between successive sectors $[E_1(S^z+1) - E_1(S^z)]\lambda$. These differences are symmetric with respect to the center of each region, with symmetrically placed differences adding up to $\frac{2i+1}{\sqrt{2}}$. This is a manifestation of the hole-particle symmetry with respect to the center of the region, after the projection to the lowest-energy dimer states has been made. If these differences do not increase with S^z the magnetization step $\Delta S^z > 1$. According to the Tables 8, 9, and 10 there are $4s$ discontinuities for a specific s, with the sectors $S^z = \frac{N}{2}i + 5$ and $S^z = \frac{N}{2}(i+1) - 5$ with $i = 0, 1, \ldots, 2s-1$ never including the ground state in a magnetic field. These are sectors whose S^z value differs by 5 from the sectors $S^z = \frac{N}{2}i$, with $i = 0, 1, \ldots, 2s$. Table 11 lists the ω_{max} values for the $4s$ discontinuities in every s, with each value belonging to a pair of discontinuities.

References

[1] P. W. Fowler and D. E. Manolopoulos, *An Atlas of Fullerenes*, Oxford University Press, Oxford (1995).

[2] H. W. Kroto, *The stability of the fullerenes C_n, with $n = 24, 28, 32, 36, 50, 60$ and 70*, Nature **329**, 529 (1987), doi:10.1038/329529a0.

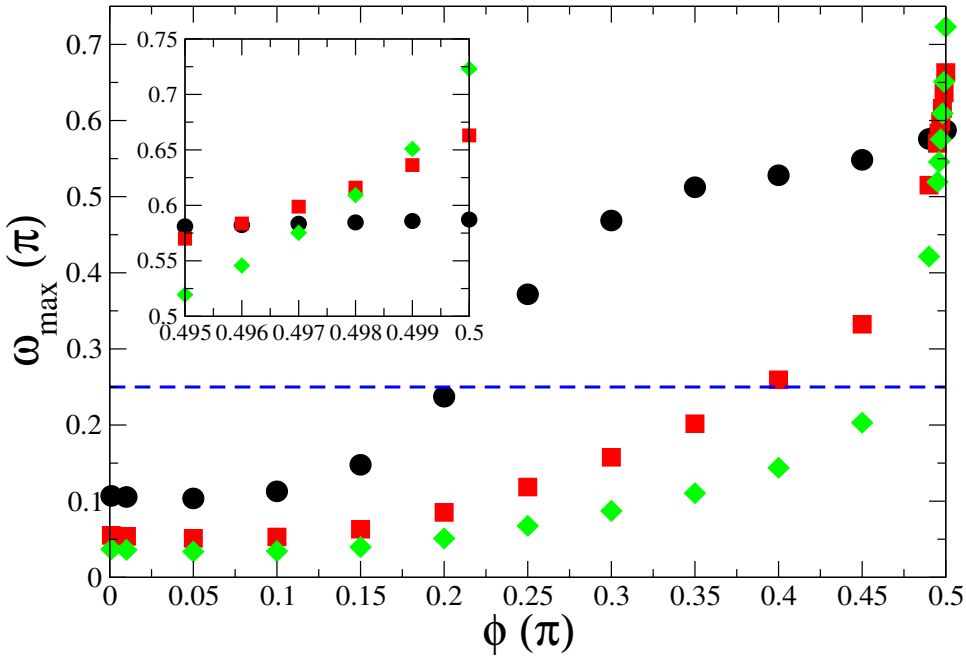

Figure 4: Maximum value ω_{max} for which the $s = \frac{1}{2}$ (black circles), 1 (red squares), and $\frac{3}{2}$ (green diamonds) ground state of Hamiltonian (1) for C_{60} has a magnetization discontinuity between $S^z = Ns - 6$ and $Ns - 4$ as a function of ϕ, which determines the relative strength of the two symmetrically independent exchange interactions. The dashed line shows the Heisenberg limit. The inset focuses on the high range of ϕ.

[3] H. W. Kroto, J. R. Heath, S. C. O'Brien, R. F. Curl and R. E. Smalley, *C_{60}: Buckminsterfullerene*, Nature **318**, 162 (1985), doi:https://doi.org/10.1038/318162a0.

[4] B. W. Smith, M. Monthioux and D. E. Luzzi, *Encapsulated C_{60} in carbon nanotubes*, Nature **396**, 323 (1998), doi:10.1038/24521.

[5] H. L. Zhang, W. Chen, L. Chen, H. Huang, X. S. Wang, J. Yuhara and A. T. S. Wee, *C_{60} Molecular Chains on α-Sexithiophene Nanostripes*, Small **3**, 2015 (2007), doi:10.1002/smll.200700381.

[6] A. Tamai, W. Auwärter, C. Cepek, F. Baumberger, T. Greber and J. Osterwalder, *One-dimensional chains of C_{60} molecules on Cu(2 2 1)*, Surf. Sci. **566**, 633 (2004), doi:10.1016/j.susc.2004.06.127.

[7] C. Zeng, B. Wang, B. Li, H. Wang and J. G. Hou, *Self-assembly of one-dimensional molecular and atomic chains using striped alkanethiol structures as templates*, Appl. Phys. Lett. **79**, 1685 (2001), doi:10.1063/1.1402648.

[8] C. Chen, H. Zheng, A. Mills, J. R. Heflin and C. Tao, *Temperature Evolution of Quasi-one-dimensional C_{60} Nanostructures on Rippled Graphene*, Sci. Rep. **5**, 14336 (2015), doi:10.1038/srep14336.

[9] N. A. Modine and E. Kaxiras, *Variational Hilbert-space-truncation approach to quantum Heisenberg antiferromagnets on frustrated clusters*, Phys. Rev. B **53**, 2546 (1996), doi:https://doi.org/10.1103/PhysRevB.53.2546.

Table 7: Maximum value ω_{max} for which the $s=\frac{1}{2}$, 1, and $\frac{3}{2}$ ground state of Hamiltonian (1) for C_{60} has a magnetization discontinuity between $S^z = Ns-6$ and $Ns-4$ for different values of ϕ, which determines the relative strength of the two symmetrically independent exchange interactions. The values for $0.5\pi^-$ are found from first-order perturbation theory on the dimer limit $\omega = \frac{\pi}{2}$ (Table 11).

$\phi(\pi)$	$\omega_{max}(s=\frac{1}{2})(\pi)$	$\omega_{max}(s=1)(\pi)$	$\omega_{max}(s=\frac{3}{2})(\pi)$
0.001	0.10693	0.05497	0.03684
0.01	0.10558	0.05385	0.03598
0.05	0.10358	0.05114	0.03375
0.1	0.11293	0.05304	0.03439
0.15	0.14775	0.06311	0.03971
0.2	0.23722	0.08522	0.05109
0.25	0.37183	0.11856	0.06764
0.3	0.46865	0.15763	0.08718
0.35	0.51236	0.20175	0.11042
0.4	0.52813	0.25949	0.14385
0.45	0.54835	0.33235	0.20304
0.49	0.57578	0.51511	0.42140
0.495	0.58107	0.56995	0.51947
0.496	0.58223	0.58366	0.54571
0.497	0.58342	0.59883	0.57525
0.498	0.58464	0.61600	0.60929
0.499	0.58591	0.63632	0.65086
0.5^-	0.58723	0.66303	0.72301

[10] A. F. Hebard, M. J. Roseeinsky, R. C. Haddon, D. W. Murphy, S. H. Glarum, T. T. M. Palstra, A. P. Ramirez and A. R. Kortan, *Superconductivity at 18 K in potassium-doped C_{60}*, Nature (London) **350**, 600 (1991), doi:https://doi.org/10.1038/350600a0.

[11] N. P. Konstantinidis, *Capped carbon nanotubes with a number of ground state magnetization discontinuities increasing with their size*, J. Phys.: Condens. Matter **29**, 215803 (2017), doi:10.1088/1361-648X/aa6bd4.

[12] S. Chakravarty, M. Gelfand and S. Kivelson, *Electronic Correlation Effects and Superconductivity in Doped Fullerenes*, Science **254**, 970 (1991), doi:10.1126/science.254.5034.970.

[13] G. Stollhoff, *Anomalous electron-lattice coupling in C_{60}*, Phys. Rev. B **44**, 10998 (1991), doi:10.1103/PhysRevB.44.10998.

[14] F. Lin, E. S. Sørensen, C. Kallin and A. J. Berlinsky, *Single-particle excitation spectra of C_{60} molecules and monolayers*, Phys. Rev. B **75**, 075112 (2007), doi:10.1103/PhysRevB.75.075112.

[15] A. Jiménez-Hoyos, R. R. Rodríguez-Guzmán and G. E. Scuseria, *Polyradical Character and Spin Frustration in Fullerene Molecules: An Ab Initio Non-Collinear Hartree–Fock Study*, J. Phys. Chem. A **118**, 9925 (2014), doi:10.1021/jp508383z.

[16] D. Coffey and S. A. Trugman, *Magnetic properties of undoped C_{60}*, Phys. Rev. Lett. **69**, 176 (1992), doi:10.1103/PhysRevLett.69.176.

Table 8: First-order perturbation theory correction of the energy E_1 for the different S^z sectors of C_{60} away from the dimer limit $\phi = \frac{\pi}{2}$ at the antiferromagnetic Heisenberg limit $\omega = \frac{\pi}{4}$ of Hamiltonian (1) for $h = 0$ and $s = \frac{1}{2}$.

S^z	E_1	S^z	E_1	S^z	E_1	S^z	E_1
0	0	8	-3.37593	16	-2.17645	24	3.44460
1	$-\frac{\sqrt{2}}{8}(\sqrt{5}+1)$	9	-3.51988	17	-1.75230	25	4.55445
2	-1.12036	10	-3.61148	18	-1.25823	26	5.63228
3	-1.64789	11	-3.52543	19	-0.69700	27	6.83739
4	-2.14589	12	-3.37955	20	-0.07595	28	8.07203
5	-2.51661	13	-3.16651	21	0.72276	29	$\frac{\sqrt{2}}{8}(55-\sqrt{5})$
6	-2.91936	14	-2.88356	22	1.57382	30	$\frac{15}{2}\sqrt{2}$
7	-3.17653	15	-2.54002	23	2.48032		

[17] A. Auerbach, *Interacting Electrons and Quantum Magnetism*, Springer Verlag, New York, doi:10.1007/978-1-4612-0869-3 (1998).

[18] P. Fazekas, *Lecture Notes on Electron Correlation and Magnetism*, World Scientific, Singapore, doi:10.1142/2945 (1999).

[19] C. Lhuillier and G. Misguich, *High Magnetic Fields (Applications in Condensed Matter Physics and Spectroscopy), Lecture Notes in Physics (Springer Series) Vol. 595*, edited by C. Berthier, L. P. Levy, and G. Martinez, Springer, New York, doi:https://doi.org/10.1007/3-540-45649-X_6 (2001).

[20] G. Misguich and C. Lhuillier, *Frustrated Spin Systems*, edited by H.T. Diep, World Scientific, Singapore, doi:https://doi.org/10.1142/8676 (2003).

[21] A. P. Ramirez, *Geometrically Frustrated Matter—Magnets to Molecules*, MRS Bull. **30**, 447 (2005), doi:10.1557/mrs2005.122.

[22] J. Schnack, *Effects of frustration on magnetic molecules: a survey from Olivier Kahn until today*, Dalton Trans. **39**, 4677 (2010), doi:10.1039/B925358K.

[23] Plato, *Timaeus*.

[24] H. Prinzbach, A. Weiler, P. Landenberger, F. Wahl, J. Wörth, L. T. Scott, M. Gelmont, D. Olevano and B. v. Issendorff, *Gas-phase production and photoelectron spectroscopy of the smallest fullerene, C_{20}*, Nature **407**, 60 (2000), doi:10.1038/35024037.

[25] Z. Wang, X. Ke, Z. Zhu, F. Zhu, M. Ruan, H. Chen, R. Huang and L. Zheng, *A new carbon solid made of the world's smallest caged fullerene C_{20}*, Phys. Lett. A **280**, 351 (2001), doi:10.1016/S0375-9601(00)00847-1.

[26] Z. Iqbal, Y. Zhang, H. Grebel, S. Vijayalakshmi, A. Lahamer, G. Benedek, M. Bernasconi, J. Cariboni, I. Spagnolatti, R. Sharma, F. J. Owens, M. E. Kozlov *et al.*, *Evidence for a solid phase of dodecahedral C_{20}*, Eur. Phys. J. B **31**, 509 (2003), doi:10.1140/epjb/e2003-00060-4.

[27] N. P. Konstantinidis, *Competition between magnetic frustration and spin dimensionality in the ground state of the classical antiferromagnetic n-vector model with arbitrary n* (2022), doi:10.48550/arXiv.2207.10535.

Table 9: Same as Tab. 8 for $s = 1$.

S^z	E_1	S^z	E_1	S^z	E_1	S^z	E_1
0	0	16	-9.90661	31	10.16959	46	15.11256
1	$-\frac{\sqrt{2}}{3}(\sqrt{5}+1)$	17	-9.41163	32	9.77693	47	16.28654
2	-2.99310	18	-8.77918	33	9.42314	48	17.57092
3	-4.40984	19	-8.01996	34	9.11786	49	18.95782
4	-5.76557	20	-7.14364	35	9.03347	50	20.43860
5	-6.83962	21	-5.92341	36	8.90460	51	22.19653
6	-7.96525	22	-4.58861	37	9.00707	52	24.04421
7	-8.80401	23	-3.14716	38	9.19497	53	25.97763
8	-9.53836	24	-1.60129	39	9.46861	54	27.99649
9	-10.16605	25	0.23145	40	9.83200	55	30.24667
10	-10.67917	26	2.01260	41	10.47254	56	32.45238
11	-10.84838	27	4.07544	42	11.20696	57	34.87899
12	-10.90051	28	6.19929	43	12.04390	58	37.35409
13	-10.82584	29	$\frac{\sqrt{2}}{3}(20-\sqrt{5})$	44	12.99124	59	39.86807
14	-10.61371	30	$\frac{15}{2}\sqrt{2}$	45	14.03629	60	$30\sqrt{2}$
15	-10.27938						

[28] R. Rausch, C. Plorin and M. Peschke, *The antiferromagnetic $S = 1/2$ Heisenberg model on the C_{60} fullerene geometry*, SciPost Phys. **10**, 087 (2021), doi:10.21468/SciPostPhys.10.4.087.

[29] N. P. Konstantinidis, *Antiferromagnetic Heisenberg model on clusters with icosahedral symmetry*, Phys. Rev. B **72**, 064453 (2005), doi:10.1103/PhysRevB.72.064453.

[30] N. P. Konstantinidis, *Unconventional magnetic properties of the icosahedral symmetry antiferromagnetic Heisenberg model*, Phys. Rev. B **76**, 104434 (2007), doi:10.1103/PhysRevB.76.104434.

[31] N. P. Konstantinidis, *$s = \frac{1}{2}$ antiferromagnetic Heisenberg model on fullerene-type symmetry clusters*, Phys. Rev. B **80**, 134427 (2009), doi:10.1103/PhysRevB.80.134427.

[32] N. P. Konstantinidis, *Zero-temperature magnetic response of small fullerene molecules at the classical and full quantum limit*, J. Magn. Magn. Mater. **449**, 55 (2018), doi:10.1016/j.jmmm.2017.09.020.

[33] J. Schulenburg, A. Honecker, J. Schnack, J. Richter and H.-J. Schmidt, *Macroscopic Magnetization Jumps due to Independent Magnons in Frustrated Quantum Spin Lattices*, Phys. Rev. Lett. **88**, 167207 (2002), doi:10.1103/PhysRevLett.88.167207.

[34] J. Richter, J. Schulenburg, A. Honecker, J. Schnack and H.-J. Schmidt, *Exact eigenstates and macroscopic magnetization jumps in strongly frustrated spin lattices*, J. Phys.: Condens. Matt. **16**, 779 (2004), doi:https://doi.org/10.1088/0953-8984/16/11/029.

[35] J. Schnack, H.-J. Schmidt, A. Honecker, J. Schulenburg and J. Richter, *Exact eigenstates of highly frustrated spin lattices probed in high fields*, J. Phys. Confer. Ser. **51**, 43 (2006), doi:https://doi.org/10.1088/1742-6596/51/1/007.

Table 10: Same as Tab. 8 for $s = \frac{3}{2}$.

S^z	E_1	S^z	E_1	S^z	E_1	S^z	E_1
0	0	23	-11.04769	46	2.08329	69	43.65523
1	$-\frac{5\sqrt{2}}{8}(\sqrt{5}+1)$	24	-8.67899	47	3.37494	70	44.47147
2	-5.61564	25	-5.83354	48	4.89081	71	45.66505
3	-8.27830	26	-3.05808	49	6.61187	72	46.98738
4	-10.83625	27	0.20699	50	8.52480	73	48.44870
5	-12.90461	28	3.57675	51	10.99590	74	50.06102
6	-15.04295	29	$\frac{\sqrt{2}}{8}(51-5\sqrt{5})$	52	13.66065	75	51.80777
7	-16.70454	30	$\frac{15}{2}\sqrt{2}$	53	16.49980	76	53.59655
8	-18.19429	31	8.56781	54	19.50498	77	55.51977
9	-19.50325	32	6.62997	55	22.97068	78	57.59398
10	-20.61117	33	4.78123	56	26.36796	79	59.80719
11	-21.14082	34	3.03344	57	30.23707	80	62.14914
12	-21.47156	35	1.75747	58	34.20713	81	64.86843
13	-21.58974	36	0.41310	59	38.26630	82	67.71467
14	-21.47556	37	-0.47076	60	$30\sqrt{2}$	83	70.67810
15	-21.15379	38	-1.18859	61	42.12444	84	73.75551
16	-20.76846	39	-1.73202	62	41.88711	85	77.14699
17	-20.17553	40	-2.08180	63	41.70662	86	80.48426
18	-19.35024	41	-1.87341	64	41.59339	87	84.13303
19	-18.31239	42	-1.47315	65	41.79165	88	87.84905
20	-17.07563	43	-0.86770	66	41.93570	89	91.62191
21	-15.26061	44	-0.03803	67	42.39383	90	$\frac{135}{2}\sqrt{2}$
22	-13.24454	45	0.99192	68	42.96594		

[36] H. Nakano and T. Sakai, *The Two-Dimensional S=1/2 Heisenberg Antiferromagnet on the Shuriken Lattice -A Lattice Composed of Vertex-Sharing Triangles-*, J. Phys. Soc. Jpn. **82**, 083709 (2013), doi:10.7566/JPSJ.82.083709.

[37] H. Nakano, M. Isoda and T. Sakai, *Magnetization Process of the S = 1/2 Heisenberg Antiferromagnet on the Cairo Pentagon Lattice*, J. Phys. Soc. Jpn. **83**, 053702 (2014), doi:10.7566/JPSJ.83.053702.

[38] H. Nakano, T. Sakai and Y. Hasegawa, *Spin-Flop Phenomenon of Two-Dimensional Frustrated Antiferromagnets without Anisotropy in Spin Space*, J. Phys. Soc. Jpn. **83**, 084709 (2014), doi:10.7566/JPSJ.83.084709.

[39] R. Furuchi, H. Nakano, N. Todoroki and T. Sakai, *Magnetization process of the S = 1/2 Heisenberg antiferromagnet on the floret pentagonal lattice*, J. Phys. Commun. **5**, 125008 (2021), doi:https://doi.org/10.1088/2399-6528/ac3f7a.

[40] R. Furuchi, H. Nakano and T. Sakai, *Numerical Study of S=1/2 Heisenberg Antiferromagnet on the Floret Pentagonal Lattice*, doi:https://doi.org/10.48550/arXiv.2209.13887 (2022).

[41] C. Schröder, H.-J. Schmidt, J. Schnack and M. Luban, *Metamagnetic Phase Transition of the Antiferromagnetic Heisenberg Icosahedron*, Phys. Rev. Lett. **94**, 207203 (2005), doi:https://doi.org/10.1103/PhysRevLett.94.207203.

Table 11: Maximum value ω_{max} for which the $s = \frac{1}{2}$, 1, and $\frac{3}{2}$ first-order perturbation theory ground state of Hamiltonian (1) away from the dimer limit $\phi = \frac{\pi}{2}$ has magnetization discontinuities, where the sectors $S^z = \frac{N}{2}i + 5$ and $\frac{N}{2}(i+1) - 5$ with $i = 0, 1, \ldots, 2s-1$ never include the ground state in the external field h.

s	i	$\omega_{max}(\pi)$
$\frac{1}{2}$	0	0.58723
1	0	0.72291
1	1	0.66303
$\frac{3}{2}$	0	0.75-
$\frac{3}{2}$	1	0.75-
$\frac{3}{2}$	2	0.72301

[42] N. P. Konstantinidis, *Antiferromagnetic Heisenberg model on the icosahedron: influence of connectivity and the transition from the classical to the quantum limit*, J. Phys.: Condens. Matter **27**, 076001 (2015), doi:10.1088/0953-8984/27/7/076001.

[43] K. Karľová, J. Strečka and J. Richter, *Enhanced magnetocaloric effect in the proximity of magnetization steps and jumps of spin-1/2 XXZ Heisenberg regular polyhedra*, J. Phys.: Condens. Matter **29**, 125802 (2017), doi:10.1088/1361-648X/aa53ab.

[44] F. Mila, *Ladders in a magnetic field: a strong coupling approach*, Eur. Phys. J. B **6**, 201 (1998), doi:https://doi.org/10.1007/s100510050542.

[45] M. Jaime, V. F. Correa, N. Harrison, C. D. Batista, N. Kawashima, Y. Kazuma, G. A. Jorge, R. Stern, I. Heinmaa, S. A. Zvyagin, Y. Sasago and K. Uchinokura, *Magnetic-Field-Induced Condensation of Triplons in Han Purple Pigment $BaCuSi_2O_6$*, Phys. Rev. Lett. **93**, 087203 (2004), doi:https://doi.org/10.1103/PhysRevLett.93.087203.

[46] X.-G. Zhou, Y. Yao, Y. Matsuda, A. Ikeda, A. Matsuo, K. Kindo and H. Tanaka, *Particle-Hole Symmetry Breaking in a Spin-Dimer System $TlCuCl_3$ Observed at 100 T*, Phys. Rev. Lett. **125**, 267207 (2020), doi:https://doi.org/10.1103/PhysRevLett.125.267207.

[47] S. L. Altmann and P. Herzig, *Point-Group Theory Tables*, Oxford University Press, London (1994).

[48] P. R. Cromwell, *Polyhedra*, Cambridge University Press, Cambridge (1997).

[49] A. Machens, N. P. Konstantinidis, O. Waldmann, I. Schneider and S. Eggert, *Even-odd effect in short antiferromagnetic Heisenberg chains*, Phys. Rev. B **87**, 144409 (2013), doi:10.1103/PhysRevB.87.144409.

[50] N. P. Konstantinidis, *Discontinuous classical ground state magnetic response as an even–odd effect in higher order rotationally invariant exchange interactions*, J. Phys.: Comm. **1**, 055027 (2017), doi:10.1088/2399-6528/aa95db.